Results in Physics 43 (2022) 106058

Contents lists available at ScienceDirect

Results in Physics

journal homepage: www.elsevier.com/locate/rinp

Study of identified particle ratios using cosmic rays Monte-Carlo models in pp collisions at $\sqrt{s} = 0.9$ and 7 TeV

L.-L. Li [a], M. Ajaz [b,*], A. Atiq [c], M. Atiq [d], M. Waqas [e,*], M.U. Ashraf [f], A.M. Khubrani [g], M. Adil Khan [h], I.S. Yahia [i,j,k]

[a] Department of Basic Sciences, Shanxi Agricultural University, Jinzhong 030801, China
[b] Department of Physics, Abdul Wali Khan University Mardan, 23200 Mardan, Pakistan
[c] Department of Physics, Division of Science and Technology, University of Education, 54770 Lahore, Pakistan
[d] Institute of Physics, The Islamia University Bahawalpur, 63100 Bahawalpur, Pakistan
[e] School of Nuclear Science and Technology, University of Chinese Academy of Sciences, Beijing 100049, China
[f] National Center for Physics, Shahdra Valley Road, Islamabad 44000, Pakistan
[g] Department of Physics, Faculty of Science, Jazan University, 45142 Jazan, Saudi Arabia
[h] Department of Physics, Islamia College Peshawar, 25120 Peshawar, Pakistan
[i] Department of Physics, College of Science, King Khalid University, P.O. Box 9004, Abha 61413, Saudi Arabia
[j] Research Center for Advanced Materials Science (RCAMS), King Khalid University, P.O. Box 9004, Abha 61413, Saudi Arabia
[k] Department of Physics, Faculty of Education, Ain Shams University, Roxy, Cairo, 11757, Egypt

ARTICLE INFO

Keywords:
Identified particles ratios
MC models
pp collisions
LHC energies

ABSTRACT

Cosmic rays with high energies can be studied only by measuring the extensive air showers of particles produced in the upper atmosphere. A complete simulation is required to know the primary particle properties, which is possible by studying the modeling of hadronic particle production at the generator level. In this connection, we report the yield ratios π^-/π^+, K^-/K^+, $\bar{p}/p$ (same particles ratio), p/π, p/K, and K/π (different particles ratio) with pseudorapidity (η) in pp collisions at $\sqrt{s} = 0.9$ and 7 TeV using models being used for extensive air shower simulation. The ratios were measured at the following transverse momentum (p_T) regions; low p_T; $0 < p_T < 0.8$ GeV/c, intermediate p_T; $0.8 < p_T < 1.2$ GeV/c and high p_T; $p_T > 1.2$ GeV/c and at different pseudorapidity (η) range of $3.0 < \eta < 4.5$ and $2.5 < \eta < 4.5$. These results are then compared with the data from the LHCb experiment. The ratio of π^-/π^+ from various model predictions agrees with the measurements at both energies at almost all p_T and η regions. There is a reasonable agreement in K^-/K^+ and $\bar{p}/p$ ratios of model and experimental data at $\sqrt{s} = 900$ GeV except few p_T and η regions, in which the models do not describe the experimental data adequately. However, almost all the models fully describe the K^-/K^+ and $\bar{p}/p$ ratios at $\sqrt{s} = 7$ TeV except few p_T and η regions. Moreover, none of the models completely reproduce the different particle ratios at $\sqrt{s} = 900$ GeV, with Pythia and EPOS producing better results. On the other hand, in most cases, the models' predictions for the different particle ratios are consistent with experimental data $\sqrt{s} = 7$ TeV. These kinds of studies will certainly help tune the Monte-Carlo generators being used for the studies of the hadron productions at various energies.

Introduction

The event multiplicity and transverse momentum (p_T) dependence studies of the identified particle production in high energy pp and AA collisions is a fundamental tool to understand the similarities and differences between the small and large interacting systems.

Due to shorter lifetimes, resonances are good candidates for understanding the particle production mechanism and hadronic phase properties [1]. Soft and hard scattering processes play an essential role in the hadron production at collider energies at the partonic level. Hard scattering results in a particle with high transverse momentum, where two partons interact with a large momentum transfer. The theoretical description of such a process is explained by the calculations of perturbative Quantum Chromodynamics (pQCD) based on factorization theorem [2].

Quantum chromodynamics (QCD) reasonably explains the hadronization processes and all other underlying interactions. However, in a non-perturbative regime, it is not easy to get precise calculations.

* Corresponding authors.
E-mail addresses: ajaz@awkum.edu.pk, muhammad.ajaz@cern.ch (M. Ajaz), waqas_phy313@ucas.ac.cn (M. Waqas).

https://doi.org/10.1016/j.rinp.2022.106058
Received 26 May 2022; Received in revised form 11 October 2022; Accepted 16 October 2022
Available online 20 October 2022

Thus a phenomenological model approach to the hadronization process and hadronic interactions must be employed to understand the particle production at low p_T. Numerous different event generators [3–7] measure experimental observables based on theoretical models. To obtain more relevant experimental results, these models are then tuned or optimized from time to time. The observables include particle species distributions, multiplicities, and different kinematics, which can serve as a reference for heavy-ion collisions. Similar results using model prediction compared to experimental data can be found in Refs. [8–17].

The anti-particle-to-particle ratio study provides additional information about the particle production mechanisms and the system's evolution in pp, particularly in heavy-ion collisions [18,19]. The main inputs for tuning a model-based generator are the relative proportions of the anti-particle ratio to particles in a given kinematic region and each charged quasi-stable hadron. The ratio of anti-proton to proton is exciting from the above-said observables. The particles in the beam decay during the high-energy inelastic collisions, mainly protons, must be balanced by inserting baryons. This process will conserve the baryon number in an event known as baryon number transport. Although several models describe this transport number, the important mechanisms which cause this phenomenon are still unclear [20–25].

The breaking up of a proton resulting in the production of a di-quark is one of the possible explanations for baryon number transport. A new particle is produced due to di-quark hadronization with some value of longitudinal momentum right after the interaction. Thus, the newly created particle balances the baryon number of the incoming proton. There is a significant role expected of pomeron exchange. However, contributions from other sources, including Odderon, may exist. The existence of the Odderon has not yet been observed [25–28]. The baryon number transport can be explored experimentally by studying the anti-proton to proton ($\bar{p}/p$) ratio as a function of some suitable kinematic variable. In ultra-relativistic pp collisions, the soft particle production is sensitive to the flavor distribution within the proton, baryon number transport, and quark hadronization.

The ratio of different particle species provides additional information about the production of particles and the evolution of the system in high energy pp and particularly in heavy-ion collisions. The output of kaons in association with pions during high-energy collisions is essential because the production of the strange particle is a powerful probe to study the process of hadronization and hadronic interactions in heavy-ion and pp collisions at ultra-relativistic energies. The study of the K/π ratio in collisions at high energies is an essential observable that explains the nuclear matter's phase transition and offers an excellent illustration of pre-equilibrium dynamics, the processes of hadronization, and dynamics of the medium hadrons.

This paper presents the results from the different Monte-Carlo (MC) generators DPMJET, EPOS, Pythia, QGSJETII, and Sibyll. The results are then compared with the data from the LHCb experiment at the same energies [29]. These results includes the same particle production ratios such as π^-/π^+, K^-/K^+, $\bar{p}/p$ and different particle production ratios $(p+\bar{p})/(\pi^+ + \pi^-)$, $(K^+ + K^-)/(\pi^+ + \pi^-)$ and $(p+\bar{p})/(K^+ + K^-)$. The prompt particles that originate from the primary interactions directly or through the subsequent decay of the resonances are considered. The ratios are measured in different p_T regions, low p_T $0 < p_T < 0.8$ GeV/c, intermediate p_T; $0.8 < p_T < 1.2$ GeV/c and high p_T; $p_T > 1.2$ GeV/c as a function of pseudorapidity, η. The pseudorapidity is given by $\eta = -ln(tan\theta/2)$, where the angle θ is the polar angle made by the particles with the beam axis. For the low p_T measurements, bins of half-integer are considered for the rapidity, i.e., $3 < \eta < 4.5$ while for the high p_T, the rapidity range is $2.5 < \eta < 4.5$.

The paper is organized as follows. Section "Models and Methodology" is devoted to a brief description of the models and methodology adopted for the analysis, followed by results and discussions in Section "Results and Discussion", and concluding remarks and summary are presented in Section "Summary".

Models and methodology

This paper includes the analyzed results from various MC generators, including DPMJETIII-2019, EPOS1.99, Pythia8.307, QGSJETII-03, QGSJETII-04, and Sibyll2.3d. A total of two hundred and fifty thousand events are simulated in each case, ensuring negligible statistical errors for simulations in most cases. We strictly followed the cuts and limits in the models used to analyze the experimental data.

In this paper, the predictions of the MC generators for the same particle ratios of pions π^-/π^+, kaons K^-/K^+, protons $\bar{p}/p$ and different particle ratios p/π, p/K and K/π are analyzed and then compared to the LHCb experimental data at CERN. For pp collisions at $\sqrt{s}$ = 0.9 TeV, we have used the DPMJETIII-2019, EPOS1.99, Pythia8.307, QGSJETII-03 models while for pp collisions at $\sqrt{s}$ = 7 TeV EPOS-LHC, QGSJETII-04 and Sibyll2.3d models are used due to the reason that DPMJET and Sibyll have many similarities. We did not consider the QGSJET-01 (older version of QGSJETII-04), which implements the Quark-Gluon-String Model and is similar to QGSJET II but is based on the old parton densities and also ignores any effects of saturation. For all the models used to analyze the data in pp collisions at $\sqrt{s}$ = 7 TeV, the treatment of parton saturation is a central challenge for the extrapolation to ultrahigh energies. QGSJETII implements the detailed theoretical model of pomeron-pomeron interaction to describe saturation effects. The saturation effects for partons regarding low virtualities can be treated consistently with this scheme of pomeron interactions. For high-virtuality partons, this scheme does nothing. The theory-inspired data-tuned parametrization model EPOS can be used to simulate the saturation effects. The extrapolation to ultrahigh energy from the EPOS is correspondingly flexible. However, the ultimate solution to the problem of parton saturation is not guaranteed after these implementations, which causes large systematic uncertainties. A brief description of these models is discussed in this section.

EPOS model

EPOS, the energy-conserving multiple scattering scheme of quantum mechanical nature based on partons, splitting of parton ladders, and off-shell remnants, is the successor of the NEXUS parton model of hadronic interactions. In EPOS, a sophisticated multi-scattering scheme emphasizing high parton densities is employed. These high parton densities are highly relevant in hA or AA nuclear collisions having relatively bigger collision system sizes. The high-density effects in EPOS are addressed by considering the Pomeron-Pomeron interactions with the parton ladder splitting approach. Collective effects are then introduced after distinguishing the highly-dense core from the peripheral outer region [30]. In this model, the parton ladder of hh interactions is assumed to have a soft part parametrized in a Regge pole fashion in addition to a conventional hard part. In addition, two off-shell remnants present another source for particle production. This three-object picture helps explain the multi-strange baryon problem of usual high energy models of interactions [31].

EPOS performs consistent calculations of cross-sections and particle productions considering the energy conservation instead of other conventional parton models that do not include the effect of energy conservation implications for the cross-section calculations. The hadronic interaction model of older EPOS 1.61 performs very well compared to particle physics experimental data, specifically from RHIC and SPS at CERN [32]. However, some extensive air shower (EAS) EPOS predictions presented interesting disagreement with KASCADE data [33]. The cosmic ray experiments may compensate for the lack of accelerator data in the forward regions and provide important feedback to improve interaction models like EPOS. A higher number of muons in EAS showers predicted with EPOS 1.61 than KASCADE was attributed to enhanced production of diquark at string ends and string fragmentation. The updated EPOS 1.99 incorporated the corrections for reduced cross-section, reduced excitation probability, and inelasticity at high energies [34].

The improved version of the model includes the effect of collective hadronization in two different flow regimes. These collective effects can be studied in the thermalized matter with relatively high densities in pp collisions and small to large AA collisions. Details on upgrades and workings of EPOS-LHC and EPOS1.99 models are available in Ref. [35] and Ref. [36] respectively.

DPMJET model

In high-energy hadronic collisions, soft multi-particle production is not entirely understood in the framework of QCD, and phenomenological models like the Dual Parton Model (DPM) are generally needed for its description. DPMJET is an MC framework of the Gribov–Glauber multiple scattering formalism that can perform simulations for hh, hA, AA, γh, $\gamma\gamma$ and γA interactions ranging from a few GeV to the ultra-high energies reached by cosmic rays. It allows the calculation of total, quasi-elastic, elastic, and production cross sections for nuclear collision systems [37]. DPMJET uses a two-component dual-parton model (DPM) in which soft processes are described by Regge theory via the exchange of pomerons. In contrast, the hard processes are attributed to perturbative parton scattering. The pp interaction model accedes from PHOJET [38], and fragmentation of parton configuration is described by the PYTHIA Lund model [39].

DPMJET-III unifies the features of three event generators, DPMJET-II, PHOJET1.12, and DTUNUC-2. For example, the prominent part of DTUNUC-2 is the representation of photo-production and collisions of nucleons up to the TeV scale. At the same time, DPMJET-II describes cosmic ray interactions to the highest energies, quasi-elastic neutrino interactions, and a few baryon-stopping diagrams. DPMJET-III considers all of these features in addition to certain common aspects like Glauber–Gribov calculations of nuclear cross-sections, intranuclear cascade in the formation zone, and the treatment of excited nuclei [37]. The model is described in more detail in Ref. [37,40].

Pythia model

Pythia is designed to simulate high-energy physics processes occurring in particle collisions, e.g., at RHIC and CERN. It is one of the most commonly used programs for event generation in high-energy collisions and allied areas. It comprises coherent physics models describing events' evolution from a few body complicated processes to multi-particle complex final states. Pythia covers a wide range of hadronic interaction tools, such as a comprehensive library for complex processes, initial/final state parton shower models, methods on hard processes and parton shower matching, beam remnants, fragmentation of strings, multi-parton interactions, and particle decays. It has the advantage of using external programs via several interfaces [41].

Pythia generates an output that records initial, intermediate, and final particles generated during evolution in three stages. Firstly, the Process-Level differentiates a hard process by combining matrix element expressions and selection of phase space. Then, at Parton-Level, evolution is traced to lower scales and higher multiplicities, including parton shower effects on hard processes, multiple interactions, and the beam remnants. Finally, the Hadron-Level stage evolves partons into hadrons by including the impact of string fragmentation and resulting decays of hadrons and leptons [42].

QGSJETII model

QGSJET is a jets-based Quark-Gluon String model used in extensive air shower (EAS) simulations of hadron cascade processes of cosmic rays. The original idea behind developing the QGSJET model was that no principal distinction exists between hard and soft processes in hadron scattering. A Q_0-cutoff parameter differentiates the kinematic region where perturbative methods may be applied from the area where phenomenological models must be employed. In a unified description, QGSJET describes both soft and semi-hard parton cascades under Gribov's Reggeon Field Theory (RFT) scheme as "soft" and "semi-hard" Pomeron exchanges [43].

Optical theorem and Abramovskii Gribov Kancheli's (AGK) cutting rules are employed to calculate cross-sections for cut diagrams' final states and contributions at a high energy limit. At the final stage, particle production is realized as the hadronization of the color field strings. The cross-sections and particle production calculations for hA and AA interactions follow as a parameter-free generalization [44]. Many scattering processes generate significant non-linear interaction effects due to parton cascades overlapping at high energies and small impact parameters. In the RFT framework, these non-linear effects are incorporated as Pomeron-Pomeron interactions. The upgraded QGSJETII treats non-linear interaction effects at the fundamental level in nuclear and hadronic interactions by considering the enhanced Pomeron diagrams [7].

Sibyll model

The Sibyll model was developed to interpret the data of cosmic rays at high energy and the originated air showers resulting from these rays. It combines perturbative QCD calculations and particle production. This model also includes the multiple properties of the multiparticle production, i.e., the effect of forward particle production, the distributions of forward particles with approximate energy scaling, the pQCD predictions about the high p_T jets, and the diffractive excited state productions of the target and projectile. To understand the whole phase space regimes beyond the limit of particle colliders and predict energies are implemented in this model. The main physical concepts to understand the scattering theory general principles are also implemented in Sibyll [45–47].

This model has had many available upgraded versions since its development. The most recent version available is Sibyll2.3d which reasonably described the fixed target and the new LHC experimental data. The remnant excitations are merged explicitly to treat the forward particle production better. In string fragmentation, the anti-baryon-baryon pair production is significantly increased compared to the soft processes. The new version also implements the Goo-Walker approach [48] to the diffraction and the charm particle production. The two-channel model (excited state and ground state) from hA interactions, which results in cross-section enhancement for the dissociated projectile diffraction on nuclei, is also improved in the latest version of the model. More details of Sibyll can be seen in Ref. [47]

Results and discussion

In this Section "Results and Discussion", the analyses of the MC generators (DPMJET, EPOS, Pythia, QGSJETII, and Sibyll) predictions for the same particle ratios of pions π^-/π^+, kaons K^-/K^+, protons $\bar{p}/p$ and different particle ratios p/π, p/K and K/π are compared to the LHCb experimental data at CERN [29]. The experimental data is divided into different p_T regions (low, intermediate and high) and η bins ($3 < \eta < 4.5$, and $2.5 < \eta < 4.5$). The events are produced from above said model-based generators at $\sqrt{s} = 0.9$ TeV and $\sqrt{s} = 7$ TeV. For low p_T, the divided region is $0 < p_T < 0.8$ GeV/c, $0.8 < p_T < 1.2$ GeV/c for intermediate p_T and $p_T > 1.2$ GeV/c for high p_T. Half-integer bin of η is considered for the low p_T region i.e., $3 < \eta < 4.5$ and for the high p_T, the rapidity is $2.5 < \eta < 4.5$.

Fig. 1 (Upper three panels) shows the pseudorapidity dependence of π^-/π^+ ratio in three different p_T regions at $\sqrt{s} = 0.9$ TeV. If the ratio equals unity, the same number of particles and anti-particle are produced. The ratio is observed to be close to unity from almost all the models at the low p_T bin ($0 < p_T < 0.8$ GeV/c) and is in good agreement with the experimental data. The Pythia and QGSJET models underestimate the data at most by 10% at the intermediate rapidity bins. For the higher p_T bin; $p_T > 1.2$ GeV/c, all of the models well

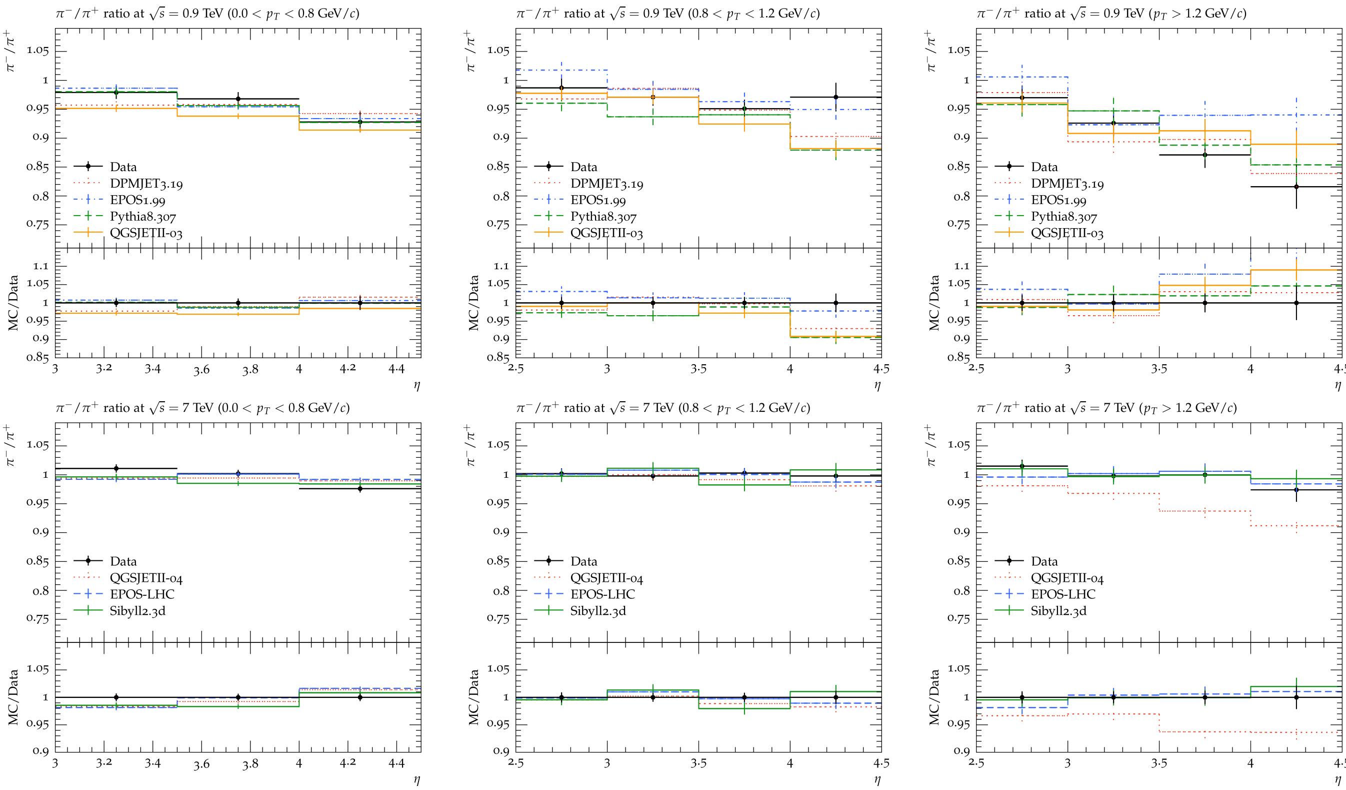

Fig. 1. (Upper three panels) The pseudorapidity dependence of π^-/π^+ ratio in three different p_T regions, low p_T; $0 < p_T < 0.8$ GeV/c, intermediate p_T; $0.8 < p_T < 1.2$ GeV/c and high p_T; $p_T > 1.2$ GeV/c by DPMJET, EPOS1.99, Pythia, and QGSJETII-03 models at $\sqrt{s}$ = 0.9 TeV. Solid markers show experimental data, while lines with different colors represent the model predictions. (Lower three panels) Same ratios are presented at $\sqrt{s}$ = 7 TeV and compared with various models. (For interpretation of the references to color in this figure legend, the reader is referred to the web version of this article.)

describe the data at low η bins within experimental uncertainties except EPOS which is off by 20% at the $4 < \eta < 4.5$ bin. The π^-/π^+ ratio is also presented with QGSJETII-04, EPOS-LHC, and Sibyll2.3d at $\sqrt{s}$ = 7 TeV in lower three panels of Fig. 1. One can observe from the figure that for the low and mid p_T bin, all models completely describe the experimental data. While for the high p_T bin, $p_T > 1.2$ GeV/c, QGSJETII-04 underestimates the particle ratio by up to about 6%, other models are in good agreement with experimental results. The experimental data and the model results show that same number of π^+ and π^- are produced at $\sqrt{s}$ = 7 TeV in all the p_T and η bins.

Fig. 2 (upper three panels) shows the pseudorapidity dependence of K^-/K^+ ratio at different p_T bins. For the low p_T bin; $0 < p_T < 0.8$ GeV/c, all models reproduce the experimental data well within the experimental and statistical errors. All models describe the data at the intermediate p_T bin; $0.8 < p_T < 1.2$ GeV/c, except at the higher η values where the DPMJET and EPOS overestimate by up to 20%. However, at the rapidity bin $\eta < 3.5$, a good agreement is observed between the experimental data and the models within the uncertainties. A different trend is seen at the high p_T bin; $p_T > 1.2$ GeV/c, where QGSJETII-03 and EPOS1.99 models are overestimating the data at high rapidity bins ($\eta > 3.5$) by 40% and 30% respectively while for rapidity bins $\eta < 3.5$, there is good agreement between the data and models. The Pythia model fully describes the experimental data for all rapidity bins within the experimental uncertainties. The DPMJET model has a good prediction of data except at the last point of η slice, where the model overestimates by 20%. Overall, the trend of the models is the same as that of the experimental data. The K^-/K^+ ratio also presented with QGSJETII-04, EPOS-LHC and Sibyll2.3d models at $\sqrt{s}$ = 7 TeV shown in lower panels of Fig. 2. All the models reasonably describe the experimental results at all the p_T bins with 5% except the low p_T bin; $0.8 < p_T < 1.2$ GeV/c, where there is a clear discrepancy between models and experimental results particularly at $\eta > 4$ where all models undershoot the data by 15%.

Fig. 3 (Upper three panels) shows the pseudorapidity dependence of $\bar{p}/p$ at different p_T bins. For the low p_T bin; $0 < p_T < 0.8$ GeV/c and rapidity bin $\eta < 3$, all the models well describe the data within the experimental uncertainties. For rapidity bin $\eta > 3$, DPMJET and QGSJETII-03 models agree well with experimental data, and the other two models, EPOS and Pythia, overestimate the data by 8% and 12% respectively. Similar behavior is observed for the intermediate p_T bin; $0.8 < p_T < 1.2$ GeV/c, where at the rapidity bin $\eta < 3$ all of the models are in agreement with the data within experimental uncertainties. For rapidity bin $\eta > 3$ Pythia overestimates the data by 20%. The DPMJET, QGSJETII-03, and EPOS1.99 models overestimate the experimental data except for the rapidity bin $\eta > 4$ where DPMJET and EPOS1.99 models reproduce the experimental data. QGSJETII-03 at the rapidity bin $\eta > 4$ underestimates the data by 12%. If we consider the uncertainties in all the cases, the discrepancy is small. At high p_T bin; $p_T > 1.2$ GeV/c, the DPMJET model is observed to reproduce the experimental data for all of the rapidity bins. EPOS1.99 and Pythia agree with data at the rapidity bin $\eta < 3$. The Pythia model overestimates the experimental data for all other rapidity bins with the highest discrepancy of about 35% for the $\eta > 4$, while EPOS1.99 reproduce the data at rapidity bin $\eta > 4$ and overestimates the data at $3 < \eta < 4$ by up to 20%. The QGSJETII-03 model agrees well with experimental data except for the rapidity bin $3.5 < \eta < 4$, which overestimates the data by 10%. The Pythia model overestimates the experimental results at all the p_T at high values of η regions. This problem is well known since only the quark-diquark breaking of the initial protons is employed by Pythia. At the same time, several authors [24,49] reported that to describe the stopping at mid-rapidity in high energy hadronic collisions, an additional mechanism is required to transport the baryon number away from the beam rapidity. Overall, all models and the experimental data observed an almost similar trend. A significant spread is also observed between the MC models and the data. The $\bar{p}/p$ ratio in comparison to

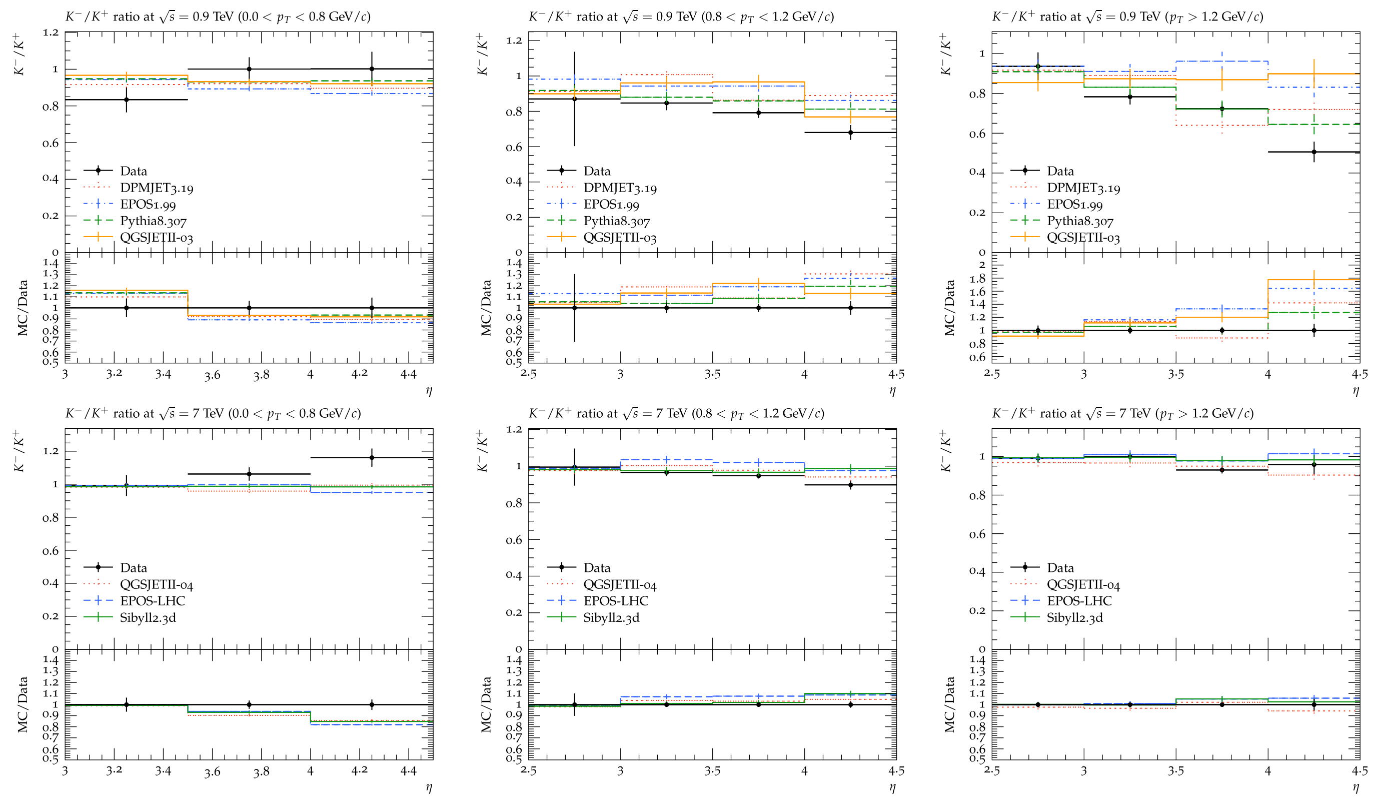

Fig. 2. (Upper three panels) The pseudorapidity dependence of K^-/K^+ ratio in three different p_T regions, low p_T; $0 < p_T < 0.8$ GeV/c, intermediate p_T; $0.8 < p_T < 1.2$ GeV/c and high p_T; $p_T > 1.2$ GeV/c by DPMJET, EPOS1.99, Pythia, and QGSJETII-03 models at $\sqrt{s} = 0.9$ TeV. Solid markers show experimental data, while lines with different colors represent the predictions from models. (Lower three panels) Same ratios are presented at $\sqrt{s} = 7$ TeV and compared with various models. (For interpretation of the references to color in this figure legend, the reader is referred to the web version of this article.)

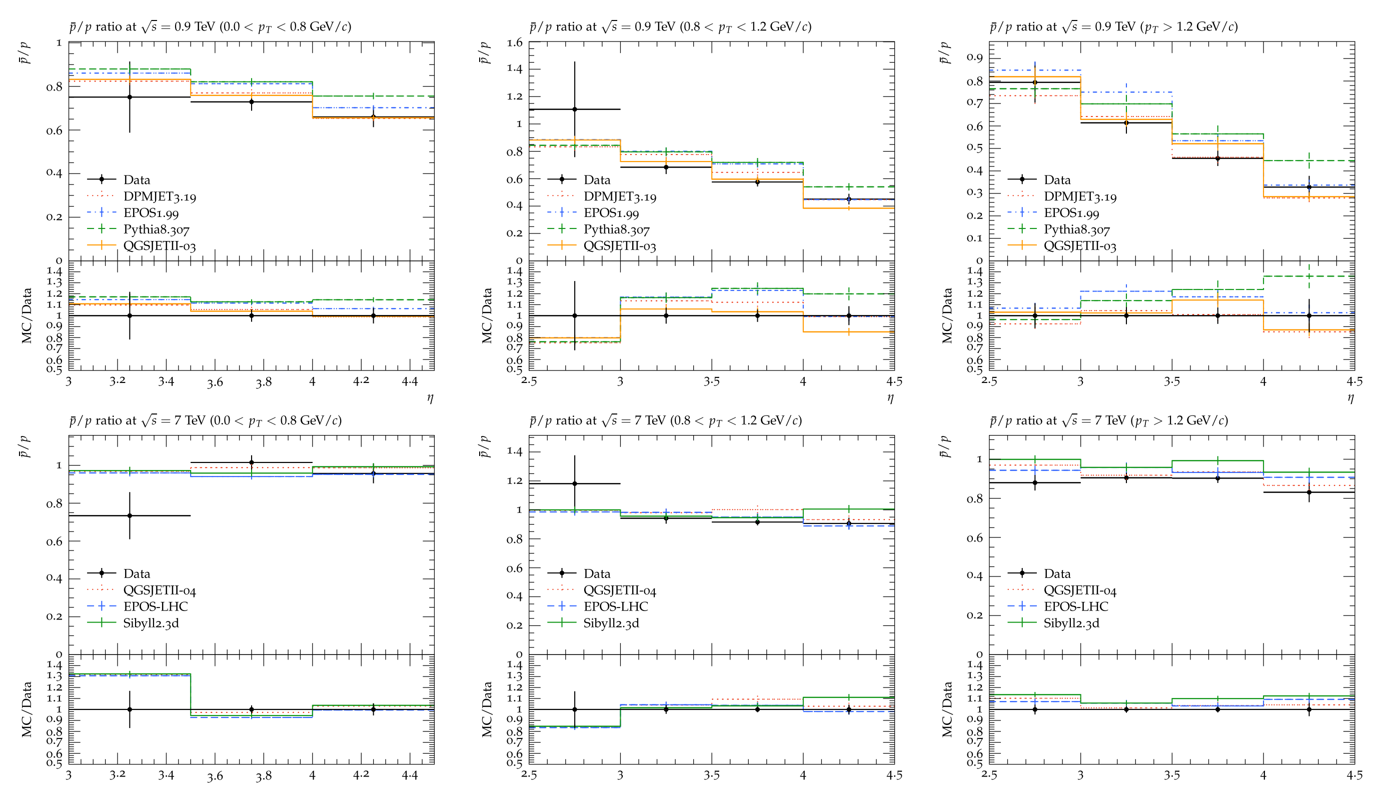

Fig. 3. (Upper three panels) The pseudorapidity dependence of $\bar{p}/p$ ratio in three different p_T regions, low p_T; $0 < p_T < 0.8$ GeV/c, intermediate p_T; $0.8 < p_T < 1.2$ GeV/c and high p_T; $p_T > 1.2$ GeV/c by DPMJET, EPOS1.99, Pythia, and QGSJETII-03 models at $\sqrt{s} = 0.9$ TeV. Solid markers show experimental data, while lines with different colors represent the predictions from models. (Lower three panels) Same ratios are presented at $\sqrt{s} = 7$ TeV and compared with various models. (For interpretation of the references to color in this figure legend, the reader is referred to the web version of this article.)

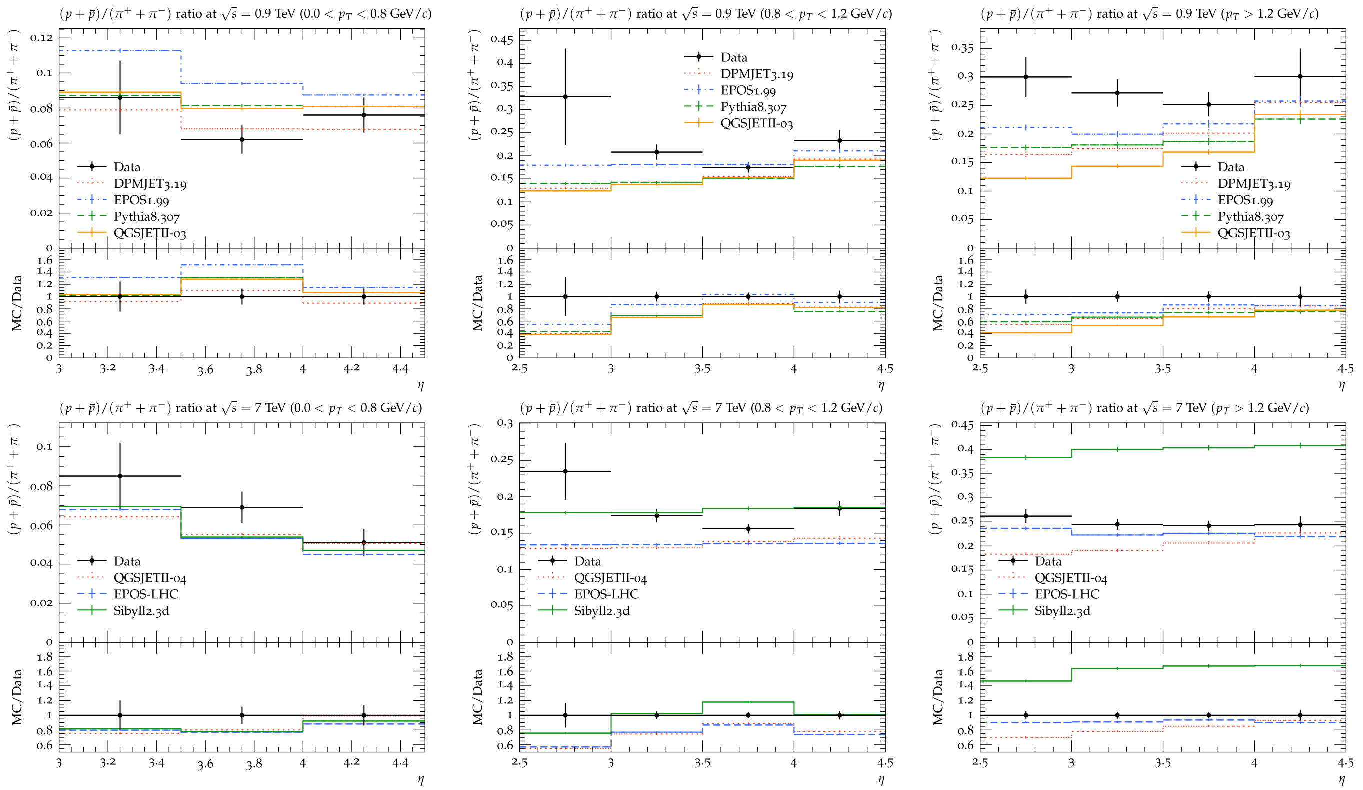

Fig. 4. (Upper three panels) The pseudorapidity dependence of p/π ratio in three different p_T regions, low p_T; $0 < p_T < 0.8$ GeV/c, intermediate p_T; $0.8 < p_T < 1.2$ GeV/c and high p_T; $p_T > 1.2$ GeV/c by DPMJET, EPOS1.99, Pythia, and QGSJETII-03 $\sqrt{s}$ = 0.9 TeV. Solid markers show experimental data, while lines with different colors represent the predictions from models. (Lower three panels) Same ratios are presented at $\sqrt{s}$ = 7 TeV and compared with various models. (For interpretation of the references to color in this figure legend, the reader is referred to the web version of this article.)

that of π^-/π^+ and K^-/K^+ ratio falls more rapidly from 0.9 at lower rapidity to around 0.3 at higher rapidity and p_T regions. We have also studied the same ratio with QGSJETII-04, EPOS-LHC, and Sibyll2.3d models at $\sqrt{s} = 7$ TeV, shown in the lower three panels of Fig. 3. These models give a good description of the experimental data within 15% for all the p_T and η regions. But none of the models fully describe the data at the whole p_T and η regime.

The pseudorapidity dependence of $(p+\bar{p})/(\pi^++\pi^-)$ ratio at different p_T bins $\sqrt{s} = 0.9$ TeV is shown in upper three panels of Fig. 4. For the low p_T bin; $0 < p_T < 0.8$ GeV/c EPOS1.99 model is observed to be overestimating the experimental data at all the rapidity bins between 10% to 40% at different η values. A good agreement between the DPMJET model and data is observed at all the rapidity bins with the experimental uncertainties. QGSJETII-03 and Pythia models reproduce the data well at the rapidity bin $\eta < 3.5$ and $\eta > 4$ while overestimating the data at the rapidity bin $3.5 < \eta < 4$ by 20%. For the intermediate p_T bin; $0.8 < p_T < 1.2$ GeV/c, QGSJETII-03, DPMJET, and Pythia models are observed to underestimate the experimental data for all of the given rapidity bins but with an increase in η the discrepancy between the models' prediction and data decreases. However, the EPOS1.99 model almost reproduces the data within the experimental uncertainties at the rapidity bin $\eta > 3$ and underestimates the experimental data at the rapidity bin $\eta < 3$ by 40%. A similar trend has been observed for the high p_T bin; $p_T > 1.2$ GeV/c, where almost all of the models underestimated the experimental data for all rapidity bins except the DPMJET and EPOS1.99 model, which are in close agreement to that of data within experimental uncertainties at the rapidity bin $\eta > 3.5$. As before, with an increase in η, the models' prediction got better. The Pythia model predicts an almost balanced ratio at a high p_T bin, similar to the experimental data distribution within uncertainties. The same ratios were also studied with QGSJETII-04, EPOS-LHC, and Sibyll2.3d models at $\sqrt{s}$ = 7 TeV and are shown in the lower three panels of Fig. 4. Compared to the models' prediction at 0.9 TeV, the prediction of models at 7 TeV is good. Sibyll reproduces the data in the low and high p_T bin within 10% but largely overpredict by a factor of up to 1.6 at the high p_T bin. EPOS-LHC results within 20% for the low and high p_T but has a discrepancy up to 40% for the intermediate p_T at $\eta < 3$. DPMJET has a similar prediction to EPOS-LHC except at the high p_T region where the discrepancy is up to 30%.

The pseudorapidity dependence of $(K^+ + K^-)/(\pi^+ + \pi^-)$ ratio at different p_T bins is shown in Fig. 5. The LHCb data shows a balanced distribution of ratios within the uncertainties. None of the models can reproduce the experimental data well for all the p_T over the whole η range. For low p_T bin; $0 < p_T < 0.8$ GeV/c, the EPOS1.99 and Pythia models agree on the data within 20% and have good predictions at the low rapidity bin $\eta < 3.5$, while it underestimates the experimental data for all other rapidity bins. Meanwhile, all the other models, QGSJETII-03 and DPMJET, underestimate the experimental data for all rapidity bins. For intermediate p_T region; $0.8 < p_T < 1.2$ GeV/c, QGSJETII-03 and DPMJET models do not reproduce the experimental data well and hence underestimate the data by up to 60%. At the rapidity bin $\eta < 3$, Pythia agrees well with only one point of the experimental data while underestimating the rest of the rapidity bins $\eta > 3$. In contrast, the EPOS1.99 model is observed to reproduce the data except at one of the rapidity bin $\eta < 3$, where the model overshoots the data by 40%. For high p_T bin; $p_T > 1.2$ GeV/c, the EPOS1.99 model reasonably reproduces the data within experimental uncertainties, following the same trend as that of the data. While the rest of the models, Pythia, DPMJET, and QGSJETII-03, underestimate with increasing discrepancy respectively and do not reproduce the experimental data at all rapidity bins. The lower three panels represent the same ratios from QGSJETII-04, EPOS-LHC, and Sibyll2.3d models at $\sqrt{s}$ = 7 TeV. The Sibyll2.3d model seems to reasonably describe the data within experimental errors and with up to 15% discrepancy at some of η bins. The EPOS-LHC

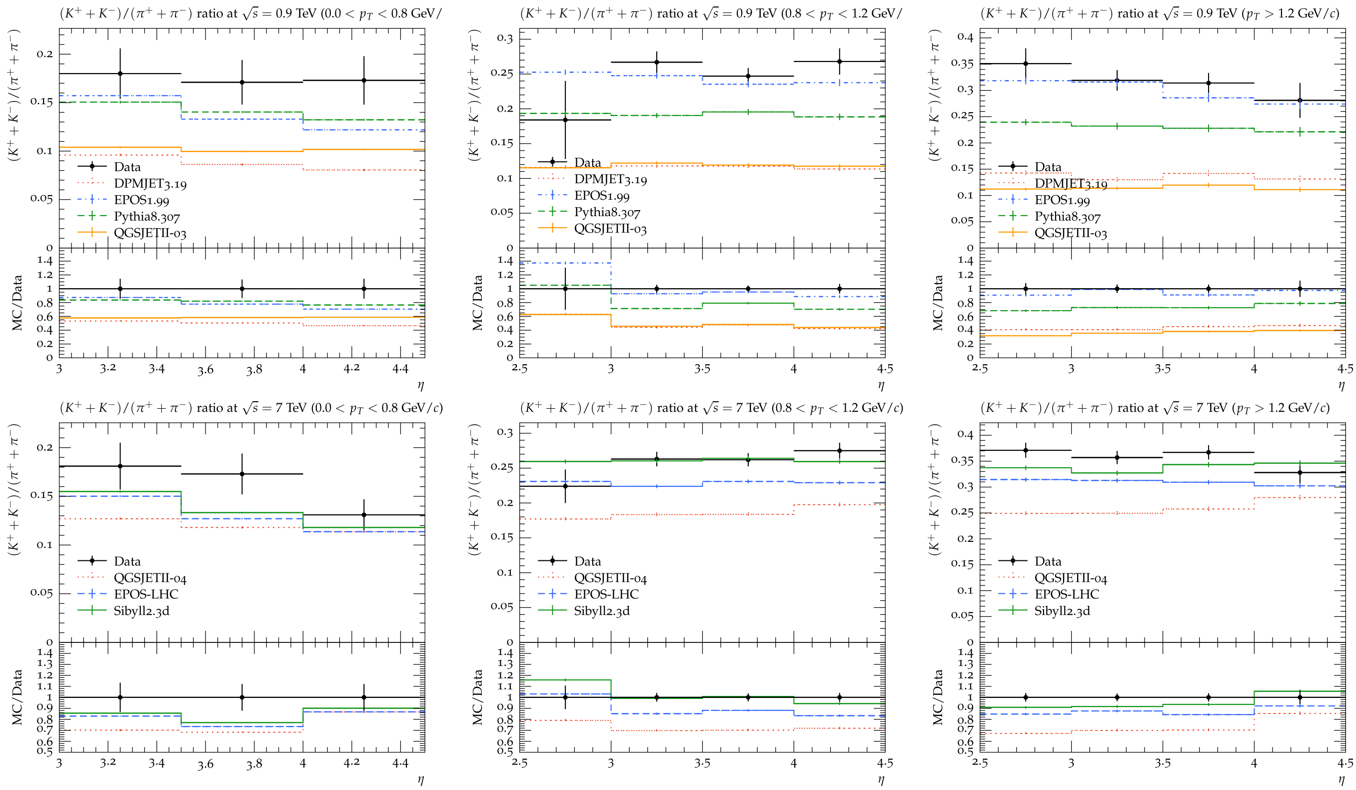

Fig. 5. (Upper three panels) The pseudorapidity dependence of K/π ratio in three different p_T regions, low p_T; $0 < p_T < 0.8$ GeV/c, intermediate p_T; $0.8 < p_T < 1.2$ GeV/c and high p_T; $p_T > 1.2$ GeV/c by DPMJET, EPOS1.99, Pythia, and QGSJETII-03 models at $\sqrt{s} = 0.9$ TeV. Solid markers show experimental data, while lines with different colors represent the predictions from models. (Lower three panels) Same ratios are presented at $\sqrt{s} = 7$ TeV and compared with various models. (For interpretation of the references to color in this figure legend, the reader is referred to the web version of this article.)

model also predicts the data within 20% discrepancy undershoots at some of the η bin in different p_T regions. Finally, the DPMJET model clearly underestimates the experimental results for all of the p_T and η regions up to 30% at $\sqrt{s} = 7$ TeV.

The pseudorapidity dependence of $(p+\bar{p})/(K^+ + K^-)$ ratio at different p_T bins is shown in Fig. 6. For low p_T bin; $0 < p_T < 0.8$ GeV/c, none of the models can reproduce the data, they all overestimate the experimental data at all of the rapidity regions except at $3 < \eta < 3.5$. For intermediate p_T region; $0.8 < p_T < 1.2$ GeV/c, Pythia and EPOS1.99 models reasonably well reproduce the data within experimental uncertainties at rapidity bins other than $2.5 < \eta < 3$ where the models underestimate the data by about 10%. QGSJETII-03 and DPMJET models do not describe, hence overestimate the data at all rapidity bins except low rapidity bin $\eta < 3$ where consistency is observed between these two models and data within the large experimental uncertainties. For high p_T bin; $p_T > 1.2$ GeV/c, QGSJETII-03 and DPMJET models do not reproduce the experimental data and hence overestimate the experimental data for all of the given rapidity bins, particularly at higher η the models are off by almost a factor of 2, while other models are within 10%. EPOS and Pythia, however, do significantly better than QGSJET and DPMJET. The lower three panels represent the same ratios from QGSJETII-04, EPOS-LHC, and Sibyll2.3d models at $\sqrt{s} = 7$ TeV. For all of the p_T and η regions, all of the models agree well with the experimental results except for a few points. However, at the high p_T bin, Sibyll is off by almost a factor of 2, while other models are within 10% of the experimental results at $\sqrt{s} = 7$ TeV. Generally, there is a good agreement between most models and experimental data at $\sqrt{s} = 7$ TeV.

Summary

We have systematically studied several models (DPMJET, EPOS1.99, Pythia8.307 and QGSJETII-03) predictions for the same particle ratios π^-/π^+, K^-/K^+, $\bar{p}/p$ and different particle ratios $(p+\bar{p})/(\pi^+ + \pi^-)$, $(K^+ + K^-)/(\pi^+ + \pi^-)$ and $(p+\bar{p})/(K^+ + K^-)$ in pp collisions at $\sqrt{s} = 0.9$ TeV and similar ratios from QGSJETII-04, EPOS-LHC and Sibyll2.3d models at $\sqrt{s} = 7$ TeV as a function of η at several p_T regions. The results are compared with the data from the LHCb experiment at CERN. A good agreement between experimental data and models has been observed in the π^-/π^+ ratio. While at some p_T regions, there is a reasonable agreement between the ratios of K^-/K^+ and $\bar{p}/p$ between models and experimental data, in others, the models do not reproduce the experimental data adequately. The Pythia model overestimates the $\bar{p}/p$ ratio in pp collisions at $\sqrt{s} = 0.9$ TeV because Pythia employs only quark-diquark breaking of the initial partons. While almost all models describe the $\bar{p}/p$ ratio in pp collisions at $\sqrt{s} = 7$ TeV. Generally, the models resulted better at 7 TeV than at 0.9 TeV.

Similarly, the models prediction of different particle ratios $(p+\bar{p})/(\pi^+ + \pi^-)$, $(p+\bar{p})/(K^+ + K^-)$, and $(K^+ + K^-)/(\pi^+ + \pi^-)$ in pp collisions at $\sqrt{s} = 0.9$ TeV and 7 TeV compared to the experimental data show a reasonable agreement in most of the p_T regions and η slices. Still, none of the models fully describes the experimental observations in all the p_T regions under consideration over the entire rapidity η range. There is no clear winner among the models, each of these does better than the others in some part of the p_T/η phase space. Hence having multiple different models is a richness for the user community. The study will help tune MC generators to study baryon production mechanisms.

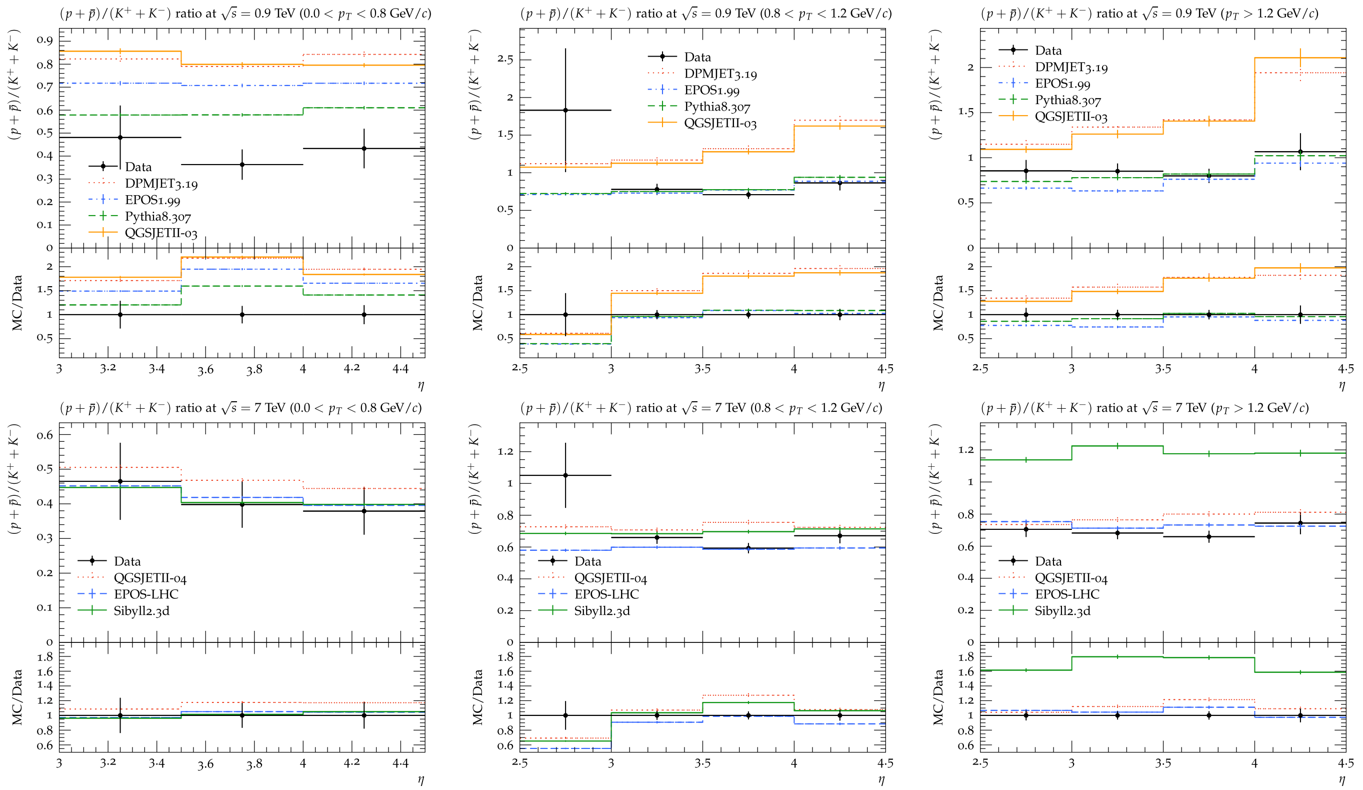

Fig. 6. (Upper three panels) The pseudorapidity dependence of p/K ratio in three different p_T regions, low p_T; $0 < p_T < 0.8$ GeV/c, intermediate p_T; $0.8 < p_T < 1.2$ GeV/c and high p_T; $p_T > 1.2$ GeV/c by DPMJET, EPOS1.99, Pythia, and QGSJETII-03 models at $\sqrt{s} = 0.9$ TeV. Solid markers show experimental data, while lines with different colors represent the predictions from models. (Lower three panels) Same ratios are presented at $\sqrt{s} = 7$ TeV and compared with various models. (For interpretation of the references to color in this figure legend, the reader is referred to the web version of this article.)

Compliance with ethical standards

The authors declare that they comply with ethical standards regarding the content of this paper.

CRediT authorship contribution statement

L.-L. Li: Wrote the main manuscript text, Reviewed the manuscript. **M. Ajaz:** Wrote the main manuscript text, Analysis, Prepared figure and interpreted the results, Reviewed the manuscript. **A. Atiq:** Analysis, Reviewed the manuscript. **M. Atiq:** Prepared figure and interpreted the results, Reviewed the manuscript. **M. Waqas:** Analysis, Prepared figure and interpreted the results, Reviewed the manuscript. **M.U. Ashraf:** Wrote the main manuscript text, Reviewed the manuscript. **A.M. Khubrani:** Analysis, Reviewed the manuscript. **M. Adil Khan:** Prepared figure and interpreted the results, Reviewed the manuscript. **I.S. Yahia:** Reviewed the manuscript.

Declaration of competing interest

The authors declare that they have no known competing financial interests or personal relationships that could have appeared to influence the work reported in this paper.

Data availability

No data was used for the research described in the article.

Acknowledgments

The authors extend their appreciation to the Deanship of Scientific Research at King Khalid University for funding this project under grant number R.G.P. 2/238/43. The authors also would like to thank the support from the Shanxi Agricultural University Ph.D. Research Startup Project under Grant No. 2021BQ103 and Shanxi Basic Research Program No.202103021223169.

References

[1] Adam J, et al., [ALICE]. Phys Rev C 2017;95(6):064606.
[2] Collins JC, Soper DE, Sterman GF. Adv Ser Direct High Energy Phys 1989;5:1–91.
[3] Sjöstrand T. Comput Phys Comm 2020;246:106910.
[4] Ostapchenko S. Phys Rev D 2011;83:014018. http://dx.doi.org/10.1103/PhysRevD.83.014018.
[5] Roesler S, Engel R, Ranft J. https://doi.org/10.1007/978-3-642-18211-2_166 [arXiv:hep-ph/0012252 [hep-ph]].
[6] Riehn F, Engel R, Fedynitch A, Gaisser TK, Stanev T. Phys Rev D 2020;102(6):063002. http://dx.doi.org/10.1103/PhysRevD.102.063002.
[7] Ostapchenko S. Nuclear Phys B Proc Suppl 2006;151:143–6. http://dx.doi.org/10.1016/j.nuclphysbps.2005.07.026.
[8] Ajaz Muhammad, Khubrani Ahmed M, Waqas Muhammad, Ismail Abd Al Karim Haj Dawi, Elmuez A. Results Phys 2022;36:105433. http://dx.doi.org/10.1016/j.rinp.2022.10543.
[9] Ullah S, Ajaz M, Wazir Z, Ali Y, Khan KH, Younis H. Sci Rep 2019;9(1):11811. http://dx.doi.org/10.1038/s41598-019-48272-4.
[10] Ajaz M, et al. Eur Phys J Plus 2022;137:52. http://dx.doi.org/10.1140/epjp/s13360-021-02271-5.
[11] Ajaz M, Haj Ismail A, Ahmed A, et al. Results Phys 2021;30:104790. http://dx.doi.org/10.1016/j.rinp.2021.104790.
[12] Yang Pei-Pin, et al. J Phys G: Nucl Part Phys 2022;49:055110. http://dx.doi.org/10.1088/1361-6471/ac5d0b.
[13] Ajaz Muhammad, et al. Results Phys 2022;36:105433. http://dx.doi.org/10.1016/j.rinp.2022.105433.
[14] Ullah S, Ajaz M, Ali Y. Europhys Lett 2018;123(3):31001. http://dx.doi.org/10.1209/0295-5075/123/31001.

[15] Ajaz M, Waqas M, Li ML-L, et al. Eur Phys J Plus 2022;137:592. http://dx.doi.org/10.1140/epjp/s13360-022-02805-5.
[16] Waqas M, Peng GX, Ajaz M, Khubrani AM, Dawi EA, Adil Khan M, et al. Results Phys 2022;42:105989. http://dx.doi.org/10.1016/j.rinp.2022.105989.
[17] Ajaz M, Haj Ismail A, Waqas M, et al. Sci Rep 2022;12:8142. http://dx.doi.org/10.1038/s41598-022-11685-9.
[18] Herrmann N, Wessels JP, Wienold T. Ann Rev Nucl Part Sci 1999;49:581–632.
[19] Satz H. Rep Progr Phys 2000;63:151.
[20] Rossi GC, Veneziano G. Nuclear Phys B 1977;123:507–45.
[21] Artru X. Nuclear Phys B 1975;85:442–60.
[22] Imachi M, Otsuki S, Toyoda F. Progr Theoret Phys 1974;52:1061.
[23] Kopeliovich BZ. Sov J Nucl Phys 1987;45:1078, JINR-E2-86-471.
[24] Kharzeev D. Phys Lett B 1996;378:238–46.
[25] Merino C, Pajares C, Ryzhinskiy MM, Shabelski YM. [arXiv:1007.3206 [hep-ph]].
[26] Lukaszuk L, Nicolescu B. Lett Nuovo Cimento 1973;8:405–13.
[27] Avila R, Gauron P, Nicolescu B. Eur Phys J C 2007;49:581–92.
[28] Csorgo T, Szanyi I. Eur Phys J C 2021;81:611. http://dx.doi.org/10.1140/epjc/s10052-021-09381-5, arXiv:2005.14319v3.
[29] Aaij R, et al., [LHCb]. Eur Phys J C 2012;72:2168.
[30] Werner K. Nuclear Phys B Proc Suppl 2008;(81–87):175–6.
[31] Liu FM, Aichelin J, Bleicher M, Drescher HJ, Ostapchenko S, Pierog T, et al. Phys Rev D 2003;67:034011.
[32] Bellwied R, [STAR]. Acta Phys Hung A 2006;27:201–4.
[33] Apel WD, et al., [Grande]. J Phys G 2009;36:035201.
[34] Pierog T, Werner K. Nuclear Phys B Proc Suppl 2009;196:102–5.
[35] Pierog T, Karpenko I, Katzy JM, Yatsenko E, Werner K. Phys Rev C 2015;92(3):034906.
[36] Pierog T. [arXiv:0906.1459 [hep-ph]].
[37] Roesler S, Engel R, Ranft J. [arXiv:hep-ph/0012252 [hep-ph]].
[38] Bopp FW, Engel R, Ranft J. Rapidity gaps and the PHOJET Monte Carlo. 1998, arXiv preprint arXiv:hep-ph/9803437.
[39] Andersson B, Gustafson G, Ingelman G, Sjöstrand T. Parton fragmentation and string dynamics. Phys Rep 1983;97(2–3):31–145. http://dx.doi.org/10.1016/0370-1573(83)90080-7, (https://www.sciencedirect.com/science/article/pii/0370157383900807).
[40] Bopp FW, Ranft J, Engel R, Roesler S. Phys Rev C 2008;77:014904.
[41] Sjöstrand T, Ask S, Christiansen JR, Corke R, Desai N, Ilten P, et al. Comput Phys Comm 2015;191:159–77.
[42] Sjöstrand T. Comput Phys Comm 2020;246:106910.
[43] Ostapchenko S. EPJ Web Conf 2013;52:02001.
[44] Ostapchenko S. AIP Conf Proc 2007;928(1):118–25.
[45] Engel J, Gaisser TK, Stanev T, Lipari P. Phys Rev D 1992;46:5013–25.
[46] Fletcher RS, Gaisser TK, Lipari P, Stanev T. Phys Rev D 1994;50:5710–31.
[47] Ahn EJ, Engel R, Gaisser TK, Lipari P, Stanev T. Phys Rev D 2009;80:094003.
[48] Good ML, Walker WD. Phys Rev 1960;120:1857–60.
[49] Capella A, Kopeliovich BZ. Phys Lett B 1996;381:325–30.